EMBO reports

scientific report

The RIG-I ATPase domain structure reveals insights into ATP-dependent antiviral signalling

Filiz Civril[1], Matthew Bennett[1], Manuela Moldt[1], Tobias Deimling[1], Gregor Witte[1,2], Stefan Schiesser[3], Thomas Carell[3,4] & Karl-Peter Hopfner[1,2,4+]

[1]Department of Biochemistry at the Gene Center, [2]Munich Center for Advanced Photonics, [3]Department of Chemistry, and [4]Center for Integrated Protein Science, Ludwig-Maximilians-University Munich, Munich, Germany

RIG-I detects cytosolic viral dsRNA with 5′ triphosphates (5′-ppp-dsRNA), thereby initiating an antiviral innate immune response. Here we report the crystal structure of superfamily 2 (SF2) ATPase domain of RIG-I in complex with a nucleotide analogue. RIG-I SF2 comprises two RecA-like domains 1A and 2A and a helical insertion domain 2B, which together form a 'C'-shaped structure. Domains 1A and 2A are maintained in a 'signal-off' state with an inactive ATP hydrolysis site by an intriguing helical arm. By mutational analysis, we show surface motifs that are critical for dsRNA-stimulated ATPase activity, indicating that dsRNA induces a structural movement that brings domains 1A and 2A/B together to form an active ATPase site. The structure also indicates that the regulatory domain is close to the end of the helical arm, where it is well positioned to recruit 5′-ppp-dsRNA to the SF2 domain. Overall, our results indicate that the activation of RIG-I occurs through an RNA- and ATP-driven structural switch in the SF2 domain.

Keywords: ATPase; crystal structure; innate immunity; RIG-I; viral RNA

EMBO *reports* (2011) **12**, 1127–1134. doi:10.1038/embor.2011.190

INTRODUCTION

The innate immune system is the first line of defence against infections by pathogens. In the innate immune system, pattern recognition receptors (PRRs) distinguish self versus non-self by binding molecular patterns that are present on pathogen-associated molecules (pathogen-associated molecular patterns (PAMPs)) but typically not on host molecules (Takeuchi & Akira, 2010). In mammals, the formation of PRR–PAMP complexes start signalling cascades that activate the transcription factors nuclear factor-κB and interferon regulatory factors, triggering host defense mechanisms such as the activation of interferon-regulated genes and inflammatory responses.

RIG-I-like receptors (RLRs) sense cytoplasmic viral RNA and comprise RIG-I, MDA5 (melanoma differentiation-associated protein 5) and LGP2 (laboratory of genetics and physiology 2; Kang *et al*, 2002; Yoneyama *et al*, 2004; Rothenfusser *et al*, 2005). RIG-I senses infections from viruses such as hepatitis C virus, Sendai virus, influenza virus, vesicular stomatitis virus, rabies virus and Japanese encephalitis virus (Kato *et al*, 2006).

After sensing RNA ligands, RIG-I associates with interferon-β promoter stimulator 1 (IPS-1), a process that involves RIG-I ubiquitination and/or interaction with ubiquitin chains (Gack *et al*, 2007; Zeng *et al*, 2010).

The optimal ligand for RIG-I has been found to be base-paired or double-stranded RNA (dsRNA) molecules containing a 5′ triphosphate (5′-ppp-dsRNA; Hornung *et al*, 2006; Pichlmair *et al*, 2006; Schlee *et al*, 2009). RIG-I contains two N-terminal caspase activation and recruitment domains (CARDs), which are required for interaction with IPS-1 (Yoneyama *et al*, 2004), a superfamily 2 helicase/translocase/ATPase (SF2) domain and a C-terminal regulatory/repressor domain (RD; Saito *et al*, 2007). The RD of RIG-I is required to activate the SF2 domain by binding 5′-ppp-RNA (Cui *et al*, 2008; Takahasi *et al*, 2008). Recent structural data show that RLR RDs are base-paired end-recognition modules with a preference for 5′-ppp-dsRNA in the case of RIG-I (Lu *et al*, 2010; Wang *et al*, 2010). However, the functional role of the SF2 domain of the RIG-I is unclear. RLRs possess the typical seven core motifs (I, Ia, II–VI) that are involved in the recognition of ATP and nucleic acid substrates (Singleton *et al*, 2007). In contrast to bona fide helicases that unwind duplex nucleic acids, RIG-I translocates on dsRNA in a 5′-ppp-dependent manner (Myong *et al*, 2009). It is unclear how dsRNA recognition by the SF2 domain and 5′-ppp recognition are linked to RIG-I activation, but current models indicate conformational changes that expose CARDs for downstream signalling (Yoneyama & Fujita, 2009).

To help reveal the mechanism of ATP-dependent RIG-I activation, we have determined the crystal structure of the mouse RIG-I SF2 domain with adenosine 5′-(β,γ-imido)triphosphate (AMP-PNP) bound.

[1]Department of Biochemistry at the Gene Center,
[2]Munich Center for Advanced Photonics,
[3]Department of Chemistry, and
[4]Center for Integrated Protein Science, Ludwig-Maximilians-University Munich, Feodor-Lynen-Strasse 25, Munich 81377, Germany
[+]Corresponding author. Tel: +49 (0) 89 2180 76953; Fax: +49 (0) 89 2180 76999; E-mail: hopfner@genzentrum.lmu.de

Received 8 September 2011; accepted 8 September 2011; published online 7 October 2011

Fig 1 | Structure of the mouse RIG-I SF2 domain. (**A**) Front view of RIG-I^{SF2} along the nucleotide-binding cleft. RIG-I^{SF2} consists of three domains: SF2 domain 1A (yellow) and SF2 domain 2A (green) are connected by a short linker helix (grey) and form the conserved ATP-binding and hydrolysis core. The helical bundle domain 2B (red) is a specific feature of RIG-I/FANCM/Hef helicases, indicating that it is involved in double-stranded nucleic acid binding or translocation. An unusual arm (orange), unique to RIG-I-like receptors, reaches from domain 2 across domain 1 and stabilizes the observed 'open' conformation. (**B**) Top view of RIG-I, coloured as in (**A**). (**C**) Close-up view of the helical arm and its elbow (orange), embracing the helical protrusion from domain 1A, with a hydrophobic interface. (**D**) Structure-based sequence alignment of selected RIG-I-like receptors with highlighted conserved residues and annotated motifs. The secondary structural elements are shown on top of the alignment. AMP-PNP, adenosine 5′-(β,γ-imido)triphosphate; RIG-I, retinoic acid inducible gene I; SF2, superfamily 2.

RESULTS

Crystal structure of the mouse RIG-I helicase domain

The SF2 domain of mouse RIG-I (mmRIG-I) was crystallized using an in-drop proteolysis approach from selenomethionine-labelled protein, and its structure determined to a resolution of 2.2 Å (which we have denoted as RIG-I^{SF2}). The structure has been deposited at the Protein Data Bank with ID 3TBK. The SF2 domain of RIG-I is a 'C'-shaped particle consisting of three structural domains denoted 1A, 2A and 2B in analogy to other SF1 and 2 enzymes (Fig 1A,B). 'RecA-like' domain 1A extends from residues 244 to 445 and carries motifs Q, I (Walker A), Ia, Ib, Ic, II (Walker B), IIa and III. It is connected to domain 2A by a short, α-helical hinge. 'RecA-like' domain 2A comprises residues 456–467 and 610–746 and carries motifs IV, V and VI (Fig 1C). 'Helical insertion' domain 2B is a compact bundle of six α-helices (α10–α15) inserted into domain 2A at the loop between β8 and α16. It is a specific feature of RLRs and the related Hef/FANCM DNA repair ATPases (supplementary Fig S3 online). Domain 2B is situated 'on top' of domain 2A, at the site that typically binds to nucleic acids in SF2 enzymes, indicating that it could be an important element of the dsRNA recognition or translocase function of RIG-I.

The three domains are connected to each other by small, mainly hydrophobic interfaces, which seem to be conserved in RIG-I, opening the possibility for conformational changes that might be important in the context of PAMP recognition and signalling. However, an unusual 'helical arm' (α18 and α19) reaches from domain 2A back to and across domain 1A. Bound to the inner side of the 'elbow' is a helical protrusion in domain 1 (α8) that interacts with both arm helices by an extended aromatic/hydrophobic interface (Fig 2A). The arm therefore seems to maintain stabilization between domains 1A and 2A in the absence of RNA in the observed conformation (which we have denoted as 'open' as described below).

Solution structure of the RIG-I helicase

To confirm that the observed 'open' state resembles the solution structure of RIG-I^{SF2}, we used small-angle X-ray scattering (SAXS) on nucleotide-free human RIG-I^{SF2}.

The scattering amplitudes measured for human RIG-I^{SF2} match those calculated from the crystal structure model of mouse RIG-I^{SF2} very well (Fig 2B). The crystal structure of mouse RIG-I^{SF2} also docks well into the averaged SAXS envelope of human RIG-I^{SF2} (Fig 2C). This shows that human RIG-I^{SF2} adopts a similar conformation in solution to mouse RIG-I^{SF2} in the crystal. We therefore propose that this conformation represents a 'signal-off' state of the RIG-I^{SF2} domain, found in the absence of an RNA ligand.

Helicase motifs and AMP-PNP recognition

The seven helicase motifs are located in loops on the surfaces of domains 1A and 2A that sandwich ATP during the ATP-hydrolysis cycle (Fig 3A). The AMP-PNP ligand is clearly defined in the electron density, bound to motif I (Fig 3B; supplementary Fig S1B online). The adenine moiety is situated in a partially polar, partially hydrophobic pocket. It is recognized by two hydrogen bonds from Q248 (Q-motif) to adenine N_6 and N_7 and by a hydrogen bond from the carbonyl oxygen of K243 to N_6. The walls of the pocket are formed by the side chains of R245, L242 and F273, providing extra stacking and hydrophobic interactions.

The β- and γ-phosphates are bound to motif I, whereas the α-phosphate lacks direct contacts (Fig 3B). The triphosphate chain appears slipped by one phosphate compared with the canonical binding; the γ-phosphate is in the position that is typically occupied by the β-phosphate. It is unclear whether this is a specific feature of RIG-I or whether conformational movements occur to allow canonical binding of the triphosphate chain.

Motif III is located in the loop that connects β6 to the α8 protrusion that binds to the helical arm. In contrast to mutations in other motifs, which abolish RIG-I activation by viral ligands, mutation of motif III was found to render RIG-I constitutively active (Bamming & Horvath, 2009), suggesting that perturbation of the protrusion–helical arm interaction might allow RIG-I activation in the absence of proper ligands.

Functional motifs are not aligned in the 'signal-off' state

Analysis of the relative location of motifs I–III and IV–VI with respect to each other shows that domain 2A needs to rotate substantially to engage domain 1A to form a functional ATPase site. For instance, motif VI residue R731 typically interacts with the triphosphate backbone, yet in the crystal structure it is ~25 Å from the γ-phosphate bound to motif I. Thus, the lack of ATPase activity in the signal-off state of RLRs can be explained by the stabilization of domains 1A and 2A in the observed 'open' orientation with misaligned helicase motifs. As we crystallized RIG-I SF2 in the presence of AMP-PNP and yet observe an 'open' structure, ATP alone is probably not sufficient to orientate the SF2 domains of RIG-I properly. In SF2 enzymes, nucleic acids are typically required to appropriately position domains 1A and 2A for ATP hydrolysis to occur. In addition, specific recognition of proper RNA ligands requires insertion domains, such as domain 2B in RIG-I^{SF2}.

To learn more about the conformational change and model how RIG-I^{SF2} might bind to RNA in an activated form, we independently superimposed RIG-I^{SF2} domains 1A and domains 2A–2B with equivalent domains 1A and 2A of the activated RNA-bound form of VASA, an SF2 DEAD box helicase with similarity to RIG-I^{SF2} (PDB 2DB3; Fig 4A; Fairman-Williams *et al*, 2010).

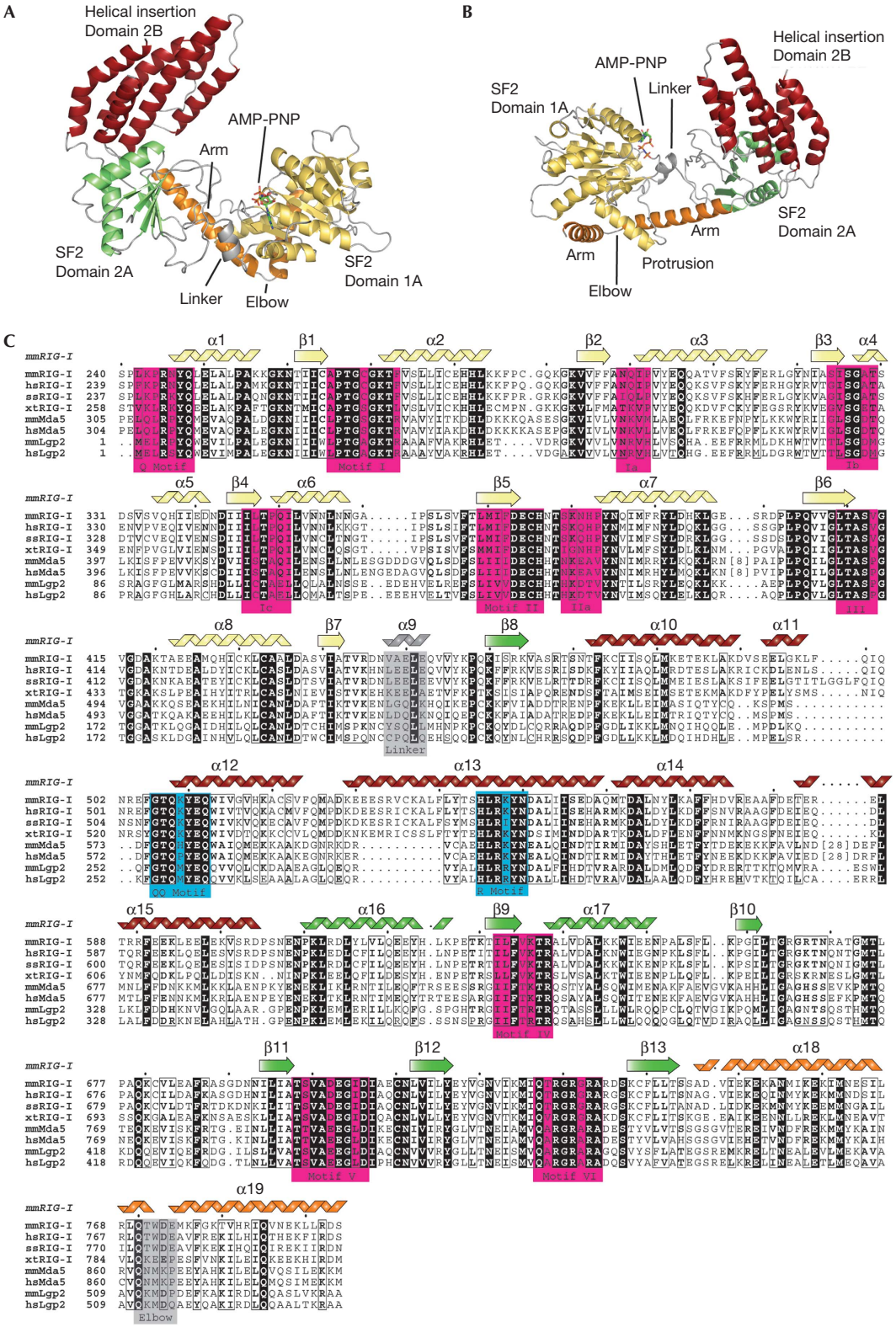

This shows that a rotation of domain 2A–2B of ~90° would properly align all motifs for activation. Notably, in the modelled 'signal-on' conformation, the helical domain 2B is situated opposite domain 1A forming a channel that is shaped to grip dsRNA (Fig 4B). The superposed conformation is also consistent with the presence of the helical arm. Although the

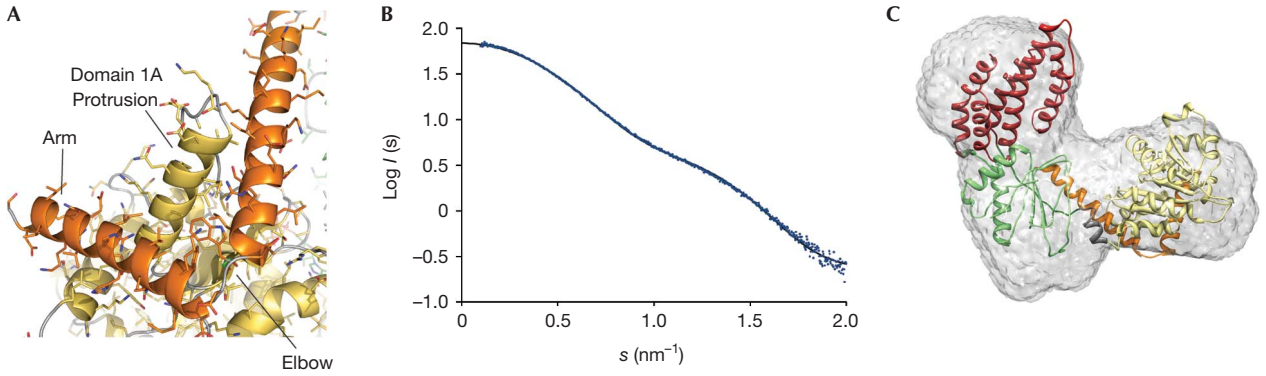

Fig 2 | Human RIG-I^{SF2} solution structure. (**A**) Experimental X-ray scattering intensities of human RIG-I^{SF2} (blue dots) and calculated scattering intensities from the crystal structure of mouse RIG-I^{SF2} (black line), indicating that the mouse RIG-I^{SF2} crystal structure is a good model for the human RIG-I^{SF2} solution structure. (**B**) Averaged small-angle X-ray scattering envelope obtained from 16 independent *ab initio* models from human RIG-I^{SF2} (grey) shows the three-lobed 'C' shape, with the model of the crystal structure of mouse RIG-I^{SF2}. Figures and docking were generated using the Situs package (Wriggers, 2010) and University of California, San Francisco Chimera (Pettersen *et al*, 2004). RIG-I, retinoic acid inducible gene I.

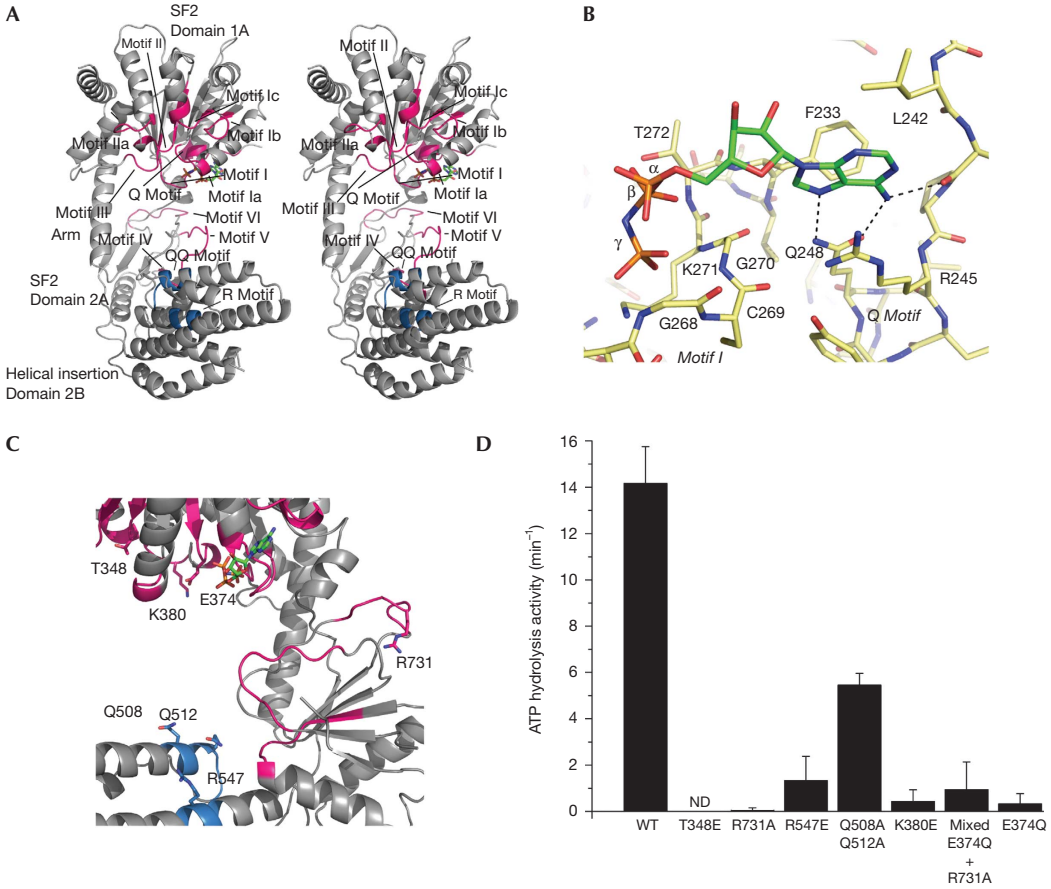

Fig 3 | Conserved motifs and mutational analysis. (**A**) Stereo view of the structure of RIG-I^{SF2} with conserved functional motifs shown. (**B**) Close-up view of the adenosine 5′-(β,γ-imido)triphosphate (AMP-PNP; colour-coded sticks: green, carbon; red, oxygen; blue, nitrogen; orange, phosphorus)-binding moiety with highlighted hydrogen bonds of the adenine recognition site. The protein is shown as colour-coded sticks with yellow carbons. (**C**) Close-up view of the motifs mutated in this study. Mutated side chains are annotated and shown as sticks. (**D**) ATP hydrolysis activity of RIG-I SF2 domain mutants. Mixed E374Q + R731A represents a 1:1 mixture of single mutants E374Q and R731A. Plotted bars: mean ± s.d. ($n = 3$–6). ND, not detectable; RIG-I, retinoic acid inducible gene I; SF2, superfamily 2; WT, wild type.

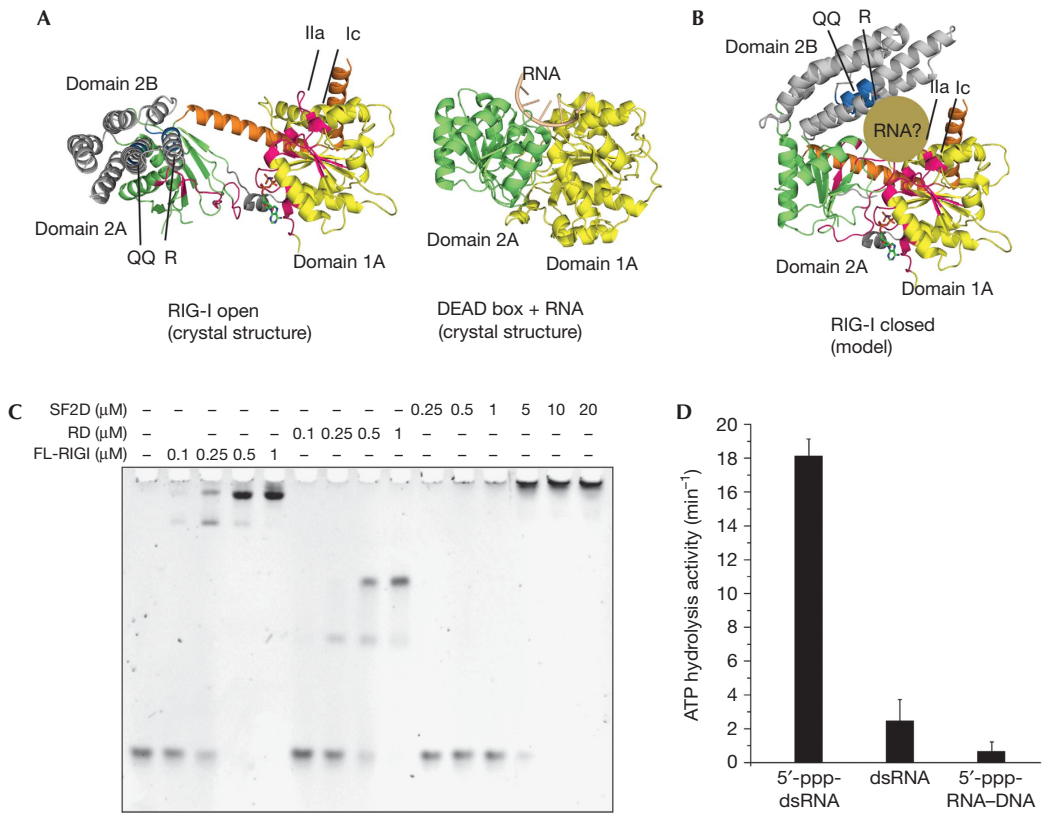

Fig 4 | Formation of an ATP hydrolysis site requires a structural switch. (**A**) Comparison of RIG-I^{SF2} (open conformation) with DEAD-box enzyme VASA (closed, RNA-bound conformation). Domains 1A are superimposed, showing the strongly differing orientation of domain 2 in RIG-I, stabilized by the helical arm. (**B**) Model of the RIG-I^{SF2} closed conformation, generated by superimposing domain 2A on the structure of VASA domain 2A. All helicase motifs align properly, and this conformation positions QQ and R motifs opposite motifs Ic and IIa, where they are ideally placed to grip dsRNA (brown). (**C**) Electrophoretic mobility shift analysis of full-length (FL) RIG-I, RD and SF2 domain (SF2D) with 5′-ppp-dsRNA. The RNA-binding affinities of RD and FL are comparable and higher than that of SF2 domain, showing that RD provides the main binding affinity of RIG-I. (**D**) ATP hydrolysis activity of RIG-I (200 nM) activated with 5′-ppp-dsRNA (25mer), dsRNA (25mer) or 5′-ppp-RNA–DNA hybrid. Plotted bars: mean ± s.d. ($n = 7$–10). dsRNA, double-stranded RNA; 5′-ppp, 5′ triphosphates; RD, repressor domain; RIG-I, retinoic acid inducible gene I; SF2, superfamily 2.

portion of domain 2A that connects to the helical arm rotates significantly, it only shifts its position by 11 Å and only modest conformational changes are required in the helical arm to accommodate this shift.

RIG-I activation requires conformational change

To understand better how RNA binding might cause a transition between the off and on states, we performed mutational analyses to locate residues important for dsRNA-stimulated ATPase activity in full-length RIG-I.

Most of the dsRNA-binding activity of RIG-I is contributed by RD (Fig 4C), which thus masks effects of mutations in SF2 in a direct RNA-binding assay (supplementary Fig S2A online). Unfortunately, without RD, SF2 alone is mostly inactive because it needs RD to present RNA for binding. However, the ATPase activity of full-length RIG-I is very sensitive to RNA-induced conformations in SF2 and can therefore help map RNA-binding motifs.

Point mutations in domain 1A motif II (E374Q) and domain 2A motif VI (R731A; Fig 3C) practically abolish 5′-ppp-dsRNA-induced ATP hydrolysis (Fig 3D), consistent with our model that these motifs must come together to form an active site. It has also been proposed that RIG-I could form multimers, in principle allowing domains 1A and 2A from different RIG-I molecules to function *in trans*, without necessitating a conformational change. However, when E374Q and R731A mutants are combined in the same reaction, ATPase activity remains diminished (Fig 3D). This lack of complementation indicates that domains 1A and 2A from the same RIG-I molecule need to come together by a conformation change to hydrolyse ATP.

Two highly conserved motifs (named QQ-motif and R-motif) form a positively charged face on the helical bundle on domain 2B (Fig 1C). In the crystal structure, these motifs are not positioned to bind RNA bound at domain 1A. However, in the model for the closed conformation (Fig 4B), the QQ- and R-motifs are repositioned opposite domain 1A in the proposed RNA-binding

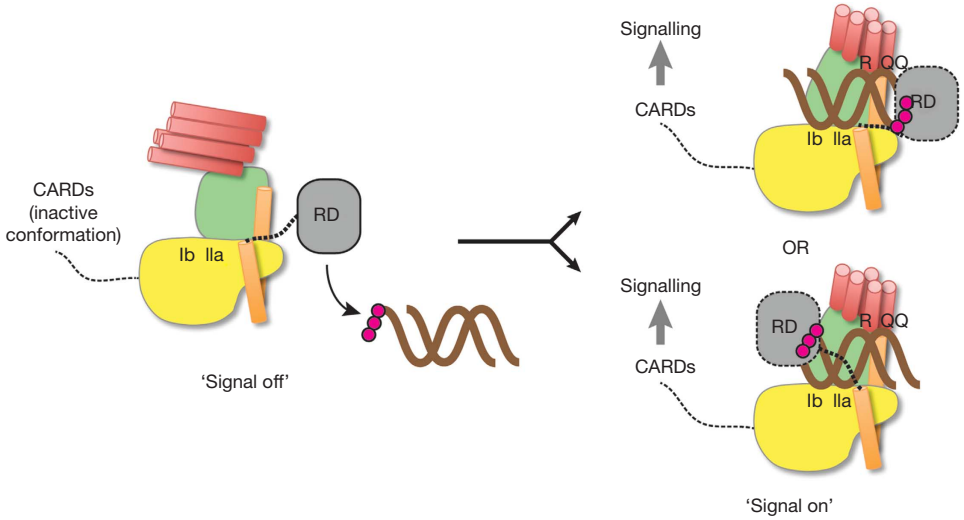

Fig 5 | Proposed model for RIG-I activation by a conformational switch in the SF2 domain. RD binds to dsRNA with 5′ triphopshates (5′-ppp; magenta spheres) and might recruit it to the SF2 domain. RNA and ATP binding switches SF2 into signal-on conformation by gripping RNA between motifs Ic/IIa on domain IA and R/QQ on domain IIB. The position of the helical arm with the short linker to RD might allow RD to bind 5′-ppp-RNA ends cooperatively with SF2. The precise position of RD, which from our structure might bind on either side of the RNA duplex (both possibilities are shown), and the position of activation and recruitment domains (CARDs) in signal-off and -on states, remain to be determined. dsRNA, double-stranded RNA; RD, repressor domain; RIG-I, retinoic acid inducible gene I; SF2, superfamily 2.

cleft. To test the relevance of these motifs, we mutated R 547 to glutamate and Q508/Q512 to alanine, and found ATPase activity reduced to ~10% and 40%, respectively (Fig 3D). The mutants retained RNA-binding activity (supplementary Fig S2B online), although this is probably due to the high affinity of the RD domain for RNA ligands (Fig 4C).

Swi/Snf2 helicases, in addition to sharing significant homology with RLRs (Fairman-Williams *et al*, 2010), are also stimulated by double-stranded nucleic acids and translocate on dsDNA by ATP-dependent tracking of the minor groove. Binding to dsDNA occurs through motifs Ia, Ib and Ic, recognizing the 3′→5′ strand, and IIa (recognizing the 5′→3′ strand; Durr *et al*, 2005).

This functional and sequence similarity between RIG-I and Swi2/Snf2 enabled us to analyse the recognition of nucleic acid duplexes by motifs Ic and motif IIa (T 348 and K 380, respectively; Fig 3C). To test the functional relevance of these motifs, we mutated T 348 and K 380 to glutamate. Both mutations abolished 5′-ppp-RNA-stimulated ATPase activity of full-length mmRIG-I (Fig 3D). As these residues are involved in nucleic acid binding in Swi/Snf2, it seems likely that motifs Ic and IIa are similarly involved in RNA duplex binding in RIG-I. A 5′-ppp-RNA–DNA hybrid binds to RIG-I similarly to 5′-ppp-dsRNA, but lacks the ability to induce ATP hydrolysis (Fig 4D; supplementary Fig S2C online), showing that a proper ATPase site is only formed when both strands of the ligand are RNA.

A model for RIG-I activation by RNA binding

Our structure, together with mutational analyses, shows how the SF2 domain of RIG-I could function as an RNA ligand-induced activation switch (Fig 5).

Interestingly, as there are only nine residues between the last structurally defined residue in RIG-I^{SF2} and the first structurally defined residues in RIG-I RD (missing in our structure), we can also roughly position RD with respect to an RNA ligand (Fig 5).

Our structure therefore provides a high-resolution framework for the signal-off state of the SF2 domain and a plausible mechanistic model for a signal-off to signal-on switch. The conservation of all motifs and the helical arm in MDA5 and LGP2 indicates that the structural model presented here is also a good framework to understand and analyse these other RLRs.

METHODS

Crystallization and structure determination. For protein purification and crystallization conditions see supplementary information online. Selenomethionine-labelled RIG-I^{SF2} was crystallized from ΔRD–RIG-I in complex with ANP-PNP using an in-drop proteolysis approach with subtilisin, which generated an SF2 helicase core with two internal loops removed (supplementary Fig S1A online). X-ray diffraction data were collected at Swiss Light Source (SLS) at the X06SA beamline at 100 K and a wavelength of 0.97972 Å (Se peak). Phenix.autosol (Terwilliger *et al*, 2009) was used to locate Se sites and produce a solvent-flattened map (supplementary Fig S1B online). A model was built using Phenix.autobuild (Adams *et al*, 2010). The model was manually improved using Coot (Emsley *et al*, 2010) and refined using Phenix.refine to an R_{work}/R_{free} of 19.1%/23.3%. Data and model statistics are shown in Table 1. The structure has been deposited at the Protein Data Bank with ID 3TBK.

Small-angle X-ray scattering. Small-angle X-ray scattering experiments were conducted at the The European Molecular Biology Laboratory/Deutsches Electronen-Synchotron X33 beamline. All proteins used were purified by size-exclusion chromatography before SAXS measurements, with running buffer used as reference. Data were processed and analysed using the ATSAS package

Table 1|Data collection and refinement statistics

Data collection	
Space group	$P2_12_12_1$
Cell dimensions	
a, *b*, *c* (Å)	45.98 86.21 152.77
α, β, γ (deg)	90, 90, 90
Resolution (Å)	50.0–2.14 (2.27–2.14)*
R_{sym}	10.2% (46.3%)
$I/\sigma I$	16.09 (3.35)
Completeness	99.4% (96.5%)
Redundancy	5.5 (5.2)
Phasing	
Figure of merit	0.47
Correlation coefficient	11.9
Refinement	
Resolution (Å)	43.89–2.14 (2.2–2.14)
No. of reflections	34,468
R_{work}/R_{free}*	19.1/23.3 (20.9/27.9)
No. of atoms	
Protein	4,182
Ligand/ion	35
Water	311
B-factors	
Protein	32.74
Ligand/ion	28.53
Water	35.28
R.m.s. deviations	
Bond lengths (Å)	0.006
Bond angles (deg)	0.912
Ramachandran values	
Favoured	98.6%
Allowed	1.4%
Outliers	0%
Protein Data Bank accession code	3TBK

*Values in parentheses are for highest-resolution shell.

(Konarev *et al*, 2006) as described in Putnam *et al* (2007). Theoretical scattering curves were calculated using CRYSOL (Svergun *et al*, 1995). Sets of independent *ab initio* models were calculated using GASBOR, and then averaged and aligned using DAMAVER (Volkov & Svergun, 2003). Figures including docking were generated using the Situs-Package (Wriggers, 2010) and UCSF Chimera (Pettersen *et al*, 2004).

RNA and DNA oligonucleotides. HPLC-grade RNA and DNA oligonucleotides were purchased from Biomers. The forward sequence used in this study is 5′-ACCAAACAAGAGAAGA AACAUGUAC-3′. 5′-ppp-RNA was synthesized as previously described (Ludwig & Eckstein, 1989; Paul *et al*, 2006) and purified by C_{18} reverse-phase chromatography at 94% purity confirmed by capillary electrophoresis.

ATPase assay. The reactions were performed in 100 mM Tris–HCl (pH 8.0), 150 mM NaCl, 10 μM $ZnCl_2$, 5 mM $MgCl_2$, 2% glycerol and 2 mM dithiothreitol (DTT). Increasing concentrations (25 nM–0.5 μM) of proteins were incubated with 1 μM *in vitro*-synthesized 5′-ppp-dsRNA, unless otherwise indicated, and 100 μM ATP including 10 nM of [γ-^{32}P]ATP for 30 min at 37 °C. Free phosphate was separated by thin-layer chromatography. Images were analysed with ImageJ. Only the linear part of the concentration curve was used for calculations.

Electrophoretic mobility shift assay. A measure of 200 nM RNA was incubated with the indicated amount of purified protein for 30 min on ice in 20 mM Tris–HCl (pH 8.0), 150 mM NaCl, 10 μM $ZnCl_2$ and 2 mM DTT reaction buffer. Samples were separated by native PAGE and stained with Gel-Red (Biotium). Gel images were analysed by ImageJ.

Supplementary information is available at EMBO *reports* online (http://www.emboreports.org).

ACKNOWLEDGEMENTS

We thank Sheng Cui for discussions and valuable support during the early phase of these studies. We thank the Max-Planck-Crystallization Facility, Martinsried, for initial screening for crystallization conditions and the staff of the Swiss Light Source (SLS; Villigen, Switzerland), The European Molecular Biology Laboratory/Deutsches Electronen-Synchotron (EMBL/DESY; Hamburg, Germany) and European Synchrotron Radiation Facility (ESRF; Grenoble, France) for excellent support. This work was funded by the National Institutes of Health grant U19AI083025 and grants from the Deutsche Forschungsgemeinschaft (DFG HO2489/3 and SFB455) to K.-P.H. K.-P.H. and T.C. acknowledge financial support by the Center for Integrated Protein Science Munich. We also acknowledge generous grants of beam time by DESY, SLS and ESRF.

Author contributions: F.C. purified and crystallized RIG-I^{SF2}, participated in structure determination and performed biochemical analyses. M.B. determined the structure and built the atomic model. M.M. helped with protein purification and crystal setups. T.D. purified human RIG-I^{SF2} and G.W. performed the SAXS analysis. S.S. synthesized 5′-ppp-RNA and T.C. designed and supervised the chemical synthesis. K.-P.H. designed and supervised the research on RIG-I and wrote the manuscript.

CONFLICT OF INTEREST

The authors declare that they have no conflict of interest.

REFERENCES

Adams PD *et al* (2010) PHENIX: a comprehensive Python-based system for macromolecular structure solution. *Acta Crystallogr D Biol Crystallogr* **66**(Part 2)**:** 213–221

Bamming D, Horvath CM (2009) Regulation of signal transduction by enzymatically inactive antiviral RNA helicase proteins MDA5, RIG-I and LGP2. *J Biol Chem* **284:** 9700–9712

Cui S, Eisenacher K, Kirchhofer A, Brzozka K, Lammens A, Lammens K, Fujita T, Conzelmann KK, Krug A, Hopfner KP (2008) The C-terminal regulatory domain is the RNA 5′-triphosphate sensor of RIG-I. *Mol Cell* **29:** 169–179

Durr H, Korner C, Muller M, Hickmann V, Hopfner KP (2005) X-ray structures of the *Sulfolobus solfataricus* SWI2/SNF2 ATPase core and its complex with DNA. *Cell* **121:** 363–373

Emsley P, Lohkamp B, Scott WG, Cowtan K (2010) Features and development of Coot. *Acta Crystallogr D Biol Crystallogr* **66**(Part 4)**:** 486–501

Fairman-Williams ME, Guenther UP, Jankowsky E (2010) SF1 and SF2 helicases: family matters. *Cur Opin Struct Biol* **20:** 313–324

Gack MU *et al* (2007) TRIM25 RING-finger E3 ubiquitin ligase is essential for RIG-I-mediated antiviral activity. *Nature* **446:** 916–920

Hornung V *et al* (2006) 5′-Triphosphate RNA is the ligand for RIG-I. *Science* **314:** 994–997

Kang DC, Gopalkrishnan RV, Wu Q, Jankowsky E, Pyle AM, Fisher PB (2002) mda-5: an interferon-inducible putative RNA helicase with double-stranded RNA-dependent ATPase activity and melanoma growth-suppressive properties. *Proc Natl Acad Sci USA* **99:** 637–642

Kato H *et al* (2006) Differential roles of MDA5 and RIG-I helicases in the recognition of RNA viruses. *Nature* **441:** 101–105

Konarev PV, Petoukhov MV, Volkov VV, Svergun DI (2006) ATSAS 2.1, a program package for small-angle scattering data analysis. *J Appl Crystallogr* **39:** 277–286

Lu C, Xu H, Ranjith-Kumar CT, Brooks MT, Hou TY, Hu F, Herr AB, Strong RK, Kao CC, Li P (2010) The structural basis of 5′ triphosphate double-stranded RNA recognition by RIG-I C-terminal domain. *Structure* **18:** 1032–1043

Ludwig J, Eckstein F (1989) Rapid and efficient synthesis of nucleoside 5′-O-(1-thiotriphosphates), 5′-triphosphates and 2′,3′-cyclophosphorothioates using 2-chloro-4H-1,3,2-benzodioxaphosphorin-4-one. *J Org Chem* **54:** 631–635

Myong S, Cui S, Cornish PV, Kirchhofer A, Gack MU, Jung JU, Hopfner KP, Ha T (2009) Cytosolic viral sensor RIG-I is a 5′-triphosphate-dependent translocase on double-stranded RNA. *Science* **323:** 1070–1074

Paul N, Springsteen G, Joyce GF (2006) Conversion of a ribozyme to a deoxyribozyme through *in vitro* evolution. *Chem Biol* **13:** 329–338

Pettersen EF, Goddard TD, Huang CC, Couch GS, Greenblatt DM, Meng EC, Ferrin TE (2004) UCSF Chimera—a visualization system for exploratory research and analysis. *J Comput Chem* **25:** 1605–1612

Pichlmair A, Schulz O, Tan CP, Naslund TI, Liljestrom P, Weber F, Reis e Sousa C (2006) RIG-I-mediated antiviral responses to single-stranded RNA bearing 5′-phosphates. *Science* **314:** 997–1001

Putnam CD, Hammel M, Hura GL, Tainer JA (2007) X-ray solution scattering (SAXS) combined with crystallography and computation: defining accurate macromolecular structures, conformations and assemblies in solution. *Q Rev Biophys* **40:** 191–285

Rothenfusser S, Goutagny N, DiPerna G, Gong M, Monks BG, Schoenemeyer A, Yamamoto M, Akira S, Fitzgerald KA (2005) The RNA helicase Lgp2 inhibits TLR-independent sensing of viral replication by retinoic acid-inducible gene-I. *J Immunol* **175:** 5260–5268

Saito T, Hirai R, Loo YM, Owen D, Johnson CL, Sinha SC, Akira S, Fujita T, Gale M Jr (2007) Regulation of innate antiviral defenses through a shared repressor domain in RIG-I and LGP2. *Proc Natl Acad Sci USA* **104:** 582–587

Schlee M *et al* (2009) Recognition of 5′ triphosphate by RIG-I helicase requires short blunt double-stranded RNA as contained in panhandle of negative-strand virus. *Immunity* **31:** 25–34

Singleton MR, Dillingham MS, Wigley DB (2007) Structure and mechanism of helicases and nucleic acid translocases. *Annu Rev Biochem* **76:** 23–50

Svergun D, Barberato C, Koch MHJ (1995) CRYSOL—A program to evaluate X-ray solution scattering of biological macromolecules from atomic coordinates. *J Appl Crystallogr* **28:** 768–773

Takahasi K, Yoneyama M, Nishihori T, Hirai R, Kumeta H, Narita R, Gale M Jr, Inagaki F, Fujita T (2008) Nonself RNA-sensing mechanism of RIG-I helicase and activation of antiviral immune responses. *Mol Cell* **29:** 428–440

Takeuchi O, Akira S (2010) Pattern recognition receptors and inflammation. *Cell* **140:** 805–820

Terwilliger TC, Adams PD, Read RJ, McCoy AJ, Moriarty NW, Grosse-Kunstleve RW, Afonine PV, Zwart PH, Hung LW (2009) Decision-making in structure solution using Bayesian estimates of map quality: the PHENIX AutoSol wizard. *Acta Crystallogr D Biol Crystallogr* **65:** 582–601

Volkov VV, Svergun D (2003) Uniqueness of ab-initio shape determination in small-angle scattering. *J Appl Crystallogr* **36:** 860–864

Wang Y *et al* (2010) Structural and functional insights into 5′-ppp RNA pattern recognition by the innate immune receptor RIG-I. *Nat Struct Mol Biol* **17:** 781–787

Wriggers W (2010) Using Situs for the integration of multi-resolution structures. *Biophys Rev* **2:** 21–27

Yoneyama M, Fujita T (2009) RNA recognition and signal transduction by RIG-I-like receptors. *Immunol Rev* **227:** 54–65

Yoneyama M, Kikuchi M, Natsukawa T, Shinobu N, Imaizumi T, Miyagishi M, Taira K, Akira S, Fujita T (2004) The RNA helicase RIG-I has an essential function in double-stranded RNA-induced innate antiviral responses. *Nat Immunol* **5:** 730–737

Zeng W, Sun L, Jiang X, Chen X, Hou F, Adhikari A, Xu M, Chen ZJ (2010) Reconstitution of the RIG-I pathway reveals a signaling role of unanchored polyubiquitin chains in innate immunity. *Cell* **141:** 315–330